RASĀYAN *J. Chem.*
Vol. 19 | No. 3 | 1566-1573 | July-September | 2026
ISSN: 0974-1496 | e-ISSN: 0976-0083 | CODEN: RJCABP
http://www.rasayanjournal.com
http://www.rasayanjournal.co.in

SIMPLE PHOSPHORIC ACID-EXTRACTION OF LATERITE MINERALS AND DOPING OF TRANSITION METALS ON NICKEL HYDROXIDES

D.K. Walanda[1,✉], M. Napitupulu[1], D. Poba[1], Y. Nurmayanti[1], Reny[1], and S.W. Donne[2]

[1]Department of Chemistry, Tadulako University, Palu-94119, Central Sulawesi, Indonesia
[2]Discipline of Chemistry, The University of Newcastle, Callaghan 2308, NSW, Australia
✉Corresponding author: walanda@gmail.com

ABSTRACT

This research investigates an efficient phosphoric acid extraction for producing nickel hydroxide battery components directly from lateritic ore. A Taguchi analysis-optimised phosphoric acid-based leaching technique quickly and easily removes nickel. Once the nickel is taken out, it is used to create β-$Ni(OH)_2$ via co-precipitation with copper or zinc (1–20%). A complete X-ray diffraction investigation indicates that doping exerts varying impacts on the structure. Adding Cu at low concentrations (≤10%) slowly raises microstrain, while adding Zn lowers it. This indicates that the two elements react with flaws in distinct ways. At 20% doping, both components show a clear barrier. This high concentration causes a lot of damage to the lattice, as seen by the very high microstrain values (for example, ~171 for Zn) and the development of additional low-angle diffraction peaks. These traits point to the fact that the solid-solution limit has been broken, which has led to phase segregation and the formation of secondary phases such as layered double hydroxides or separate metal hydroxides. The study reveals that phosphoric acid is a good leaching agent and that modified nickel hydroxides can only be doped with less than 10% of it to stay stable. This is a simple approach to change the materials of alkaline batteries from a mineral source that may be used over and over again.

Keywords: Acid Leaching, Phosphoric Acid, Laterite Mineral, Transition Metal Doping, Nickel Hydroxides

RASĀYAN *J. Chem.*, Vol. 19, No.3, 2026

INTRODUCTION

Rechargeable nickel-based batteries are a key part of disruptive technology like portable devices, power tools, and electric cars that are becoming a greater option in terms of safety issues. Ni/Zn, Ni/Cd, Ni/Metal-hydride, and Ni/Hydrogen are all nickel-based batteries that fall within the category of alkaline secondary batteries.[1–3] The most important part of this category of batteries is the electroactive $Ni(OH)_2$ electrode, which is used as the positive electrode. This electrode is what makes the battery's energy density so high. Incremental improvement of synthetic methods for making electrodes, adding some ion metals, or modifying the structure of the crystal can all improve the electrochemical performance.[4–7] Nickel hydroxide exhibits two well-known phases, which are α-$Ni(OH)_2$ and β-$Ni(OH)_2$, where both polymorphs crystallise in the hexagonal system, showing a brucite-type arrangement characterised by $Ni(OH)_2$ layers arranged along the c-axis. Water molecules and alkali metal ions are interpolated between the (0 0 1) plane in the α-$Ni(OH)_2$ lattice. The unit cell's lattice parameters in the hexagonal system are c_o = 8.05 Å and a_o = 3.08 Å. The spacing between the layers of α-$Ni(OH)_2$ is roughly 0.78 nm.[8] The primary distinction between the α-$Ni(OH)_2$ and β-$Ni(OH)_2$ phases is in the arrangement of the strata throughout the c-axis. For α-$Ni(OH)_2$, the hexagonal layers are maintained along the c-axis with 0.46 nm between molecules. In β-$Ni(OH)_2$, the layers exhibit a reduced level of order relative to one another, which creates a turbostratic plane when water molecules and anionic species like nitrate, carbonate, and sulfate are present at the van der Waals gap. The lattice dimensions for β-$Ni(OH)_2$ in the hexagonal configuration are c_o = 4.65 Å and a_o = 3.12 Å.[9] The β-$Ni(OH)_2$ is commonly utilised as an active constituent for nickel-based cathodes. It is also widely accepted that the α-phase is more electrochemically reactive than the β-phase, probably because OH and H_2O can move more freely through the mostly separated nickel

http://doi.org/10.31788/RJC.2026.1939662
This work is licensed under a CC BY 4.0 license.

hydroxide layer.[10] Numerous methods exist to facilitate the preparation and discharge of the active material in nickel hydroxide electrodes for rechargeable nickel batteries. Since the beginning of the century, a substantial body of research has been devoted to the development of chemical and electrochemical impregnation techniques.[11-12] The hydrothermal method is a new way to make nickel hydroxide that is good for batteries.[13] Previous researchers examined the electrochemical infusion of porous nickel sintered plates to gain insights into the composition and structure of the material that was deposited.[14] A comprehensive suite of characterisation techniques, including discharge mechanism, SEM, in-situ Spectroscopy, and XRD, was employed to systematically evaluate the chemical composition and electrochemical behaviour of the α- and β-nickel hydroxide phases.[15] Various researchers led to the creation of β-$Ni(OH)_2$, whereas Le Bihan and Figlarz[17] reported a very disordered hydrated form of $Ni(OH)_2$ called turbostratic $Ni(OH)_2$. The many types of $Ni(OH)_2$ have different chemical structures,[18] levels of hydration,[19] and shapes.[20] It has been said that $Ni(OH)_2$ made with electrochemistry has better electrochemical characteristics than $Ni(OH)_2$ made with chemicals.[21] Materials featuring a high specific area, significant porosity, and small particle size are recognised for possessing enhanced charge and discharge capacities.[22] So, it is best to make nickel hydroxide that has these exact properties. One way to do this is to make nickel hydroxide fall out of solution when complexing reagents are present. A complexing agent is what controls how quickly nickel hydroxide precipitates. The International Energy Agency (IEA) report indicated that the share of nickel utilized in the energy sector rose from 6% in 2017 to 16% in 2022, a key factor fueling worldwide demand for primary nickel, along with a 60% increase in sales of nickel-based battery electric vehicles in 2022.[23] However, Fraser *et al.*[24] estimate that global primary nickel supply will decline around 2028, with a structural deficit of approximately 0.977×10^6 tons in 2040, particularly in the clean energy sector (clean energy-energy saved through energy efficiency measures). As a result, nickel for batteries has been included in the European Union's fifth edition of its list of critical raw materials in 2023.[25] Consequently, battery-grade nickel was added to the European Union's fifth Critical Raw Materials List in 2023.[25] Although Indonesia, the world's largest producer of primary nickel, has advanced its shift from nickel pig iron (NPI) to nickel matte and is developing several high-pressure acid leaching (HPAL) facilities to supply the clean energy sector,[26] this transition is not without challenges. These include increased energy requirements, while HPAL technology also raises significant environmental concerns. In this work, we present simple phosphoric acid extraction of laterite minerals and doping of transition metals (Cu and Zn) on nickel-based battery raw materials. The goal was to develop a less complex, potentially lower-temperature extraction and synthesis route that offers a more direct, potentially greener pathway from raw ore for battery materials and apply Cu/Zn doping to improve the structural stability of nickel-rich materials by modifying the nickel hydroxide with the presence of doping ions.

EXPERIMENTAL

Laterite mineral samples were obtained from laterite mineral mining/excavation sites in the Bahodopi area of Morowali Regency, Central Sulawesi, at a depth of approximately 2-3 meters from the ground surface, where the mineral texture was a mixture of clay and brown clay-colored rock.[27] The samples were then dried for 1 week under the sun and then ground and sieved using an 80-mesh sieve. Next, before the acid-leaching stage, the laterite soil samples were characterized, including morphological characterization (SEM) of laterite minerals, which can be seen in Fig.-1, while elemental characterization (EDS, Energy Dispersive X-ray Spectroscopy) can be seen in Fig.-2.[28]

Table-1: Experimental Parameters and their Levels for Acid Leaching Stage

Parameter	Level			
	1	2	3	4
H_3PO_4 concentration (M)	0.5	2.0	3.5	5.0
Temperature (°C)	30	50	70	90
Leaching time (hours)	0.5	1.0	2.0	4.0
Agitation rate (rpm)	250	500	750	1000

Nickel hydroxide samples were prepared according to the following procedures: 50 mL of nickel filtrate was added to NaOH solutions with varying concentrations (10, 15 and 20%) and other condition

parameters such as temperature (35, 45 and 55 °C) and pH (8-10), inside a flask container. The generated suspension was stirred continuously overnight. After that, the green-jelly suspension was left to settle down, where it was then filtered and was washed with distilled water. This procedure was performed three times to wash the solid material. The solid was then dried in the oven at 60 °C for 24 hours. The Williamson-Hall method was utilised to deconvolute XRD peak broadening to separately determine the effects of crystallite size and internal lattice microstrain.[29]

RESULTS AND DISCUSSION

The SEM images (Fig.-1(a-c)) captured at 500× up to 8000× magnification revealed a heterogeneous morphology characterised by irregularly shaped particles and aggregates of varying sizes, distributed unevenly across the field of view. The surface texture of the particles is notably rough, with both fine fragments and larger chunks present, suggesting a complex microstructure. The image spans average or sizes from M = 137.137; SD = 45.115 μm in Fig.-1(a) to M = 1.230; SD = 0.487 μm in Fig.-1(c), with a scale bar indicating 400 μm - 5 μm and was acquired using a CBS detector at an accelerating voltage of 5.00 and 7.00 kV and a various working distances. Such morphological features are indicative of a material with high surface area and potential for diverse physicochemical interactions, relevant in applications such as adsorption, catalysis, or soil science.

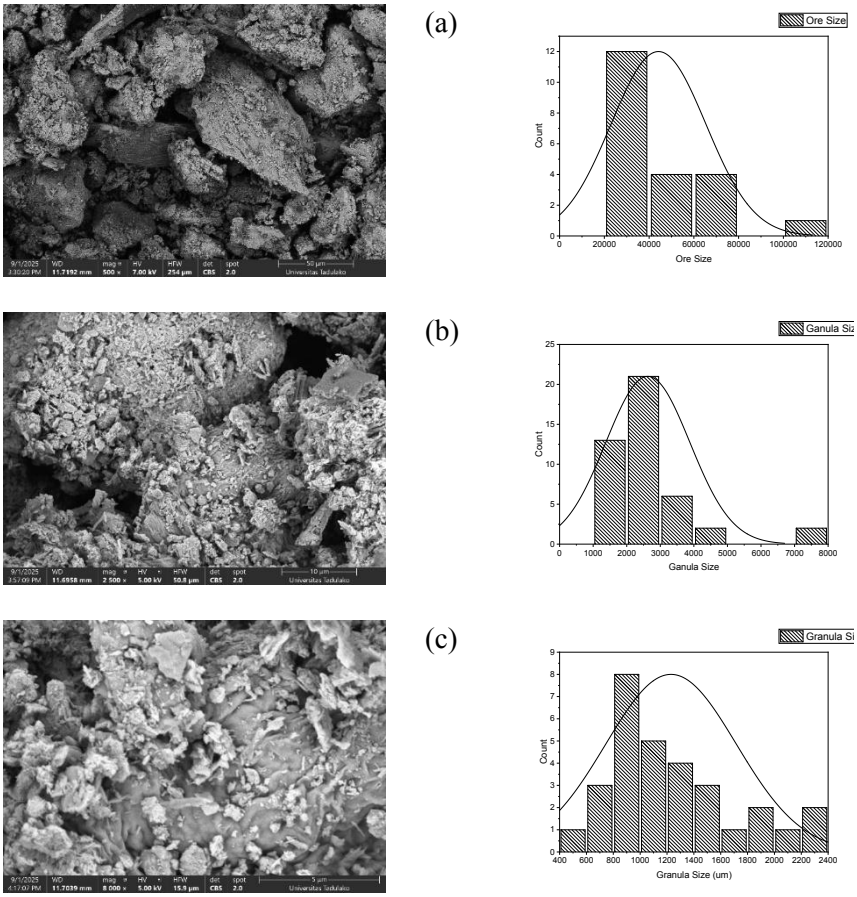

Fig.-1: Morphology of Laterite Mineral Samples and Size Distribution with Magnification Variations (a) 500x, (b) 2500x, and (c) 8000x

The energy dispersive X-ray spectroscopy (EDS) (Fig.-2) analysis of the sample reveals a diverse elemental composition, as indicated by distinct peaks in the spectrum. The presence of carbon (C) at ~0.3 keV suggests organic or carbonaceous material, while titanium (Ti) and vanadium (V) -with overlapping signals near 0.45–0.5 keV-point to possible mineral phases or metal oxides. A prominent oxygen (O)

peak supports the existence of oxides or silicates. Iron (Fe), detected around 0.7 keV, is likely a major component, possibly in the form of iron oxides or lateritic minerals. Peaks for magnesium (Mg) at ~1.25 keV and aluminium (Al) at ~1.5 keV suggest the presence of aluminosilicate minerals, while nickel (Ni) at ~2 keV may indicate trace metal content, often associated with lateritic soils. The relative intensities of these peaks provide insight into the elemental abundance, making this EDS spectrum a valuable tool for characterizing the chemical makeup and potential geochemical behaviour of the sample.

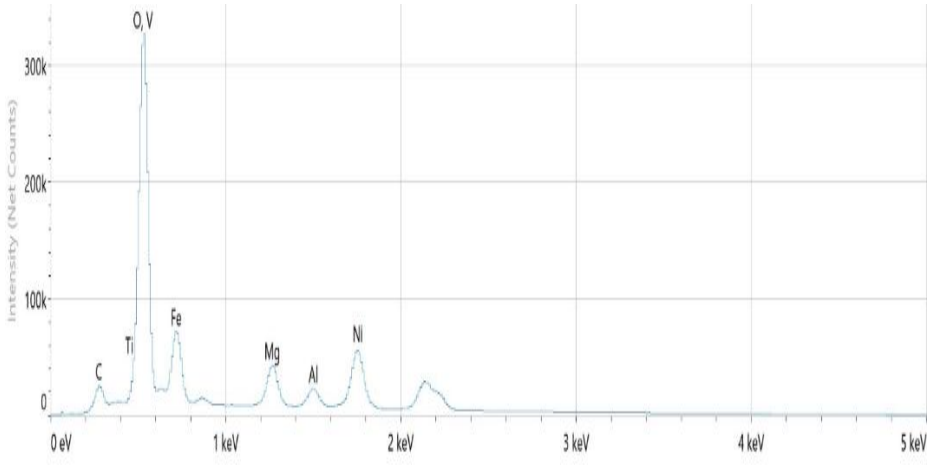

Fig.-2: Elemental Characterization Spectrum (EDS) of Laterite Mineral Samples

The main effects plot for S/N ratios in the Fig.-3 illustrates the influence of four experimental factors—H_3 PO_4 concentration (M), temperature (°C), leaching time (hours), and agitation speed (rpm)—on the signal-to-noise (S/N) ratio, following the Taguchi method with the objective of larger is better. The plot revealed that increasing H_3PO_4 concentration initially reduces the S/N ratio from 0.5 M to 2.0 M, suggesting diminished performance, but a slight recovery is observed at higher concentrations (3.5 M and 5.0 M). Temperature showed a non-linear trend, with the S/N ratio rising from 30 °C to 50 °C, dipping at 70 °C, and increasing again at 90 °C, indicating optimal leaching conditions may occur at moderate to high temperatures. Time exhibits a generally increasing trend, peaking around 1–2 hours, implying that prolonged leaching enhances performance up to a point before diminishing returns set in. Speed showed variable effects, with mid-range rpm values yielding higher S/N ratios, suggesting that moderate agitation improves leaching efficiency. Overall, the analysis helps identify optimal parameter settings for maximizing leaching performance under the Taguchi design framework.

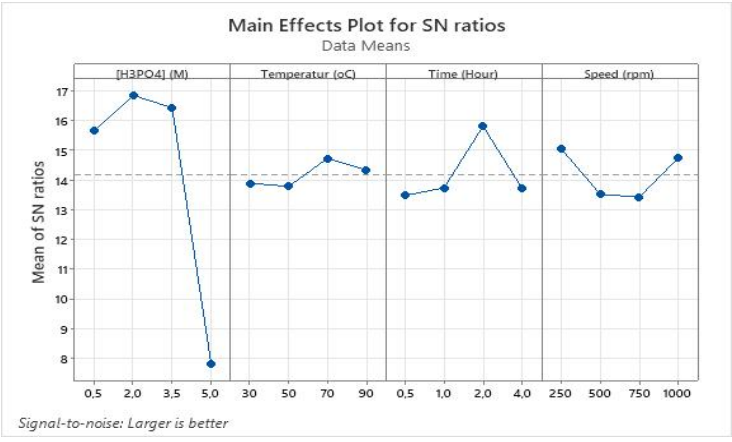

Fig.-3: Plots for Analysis Results of Acid-Leaching using the Taguchi Method with the Larger is Better S/N Option

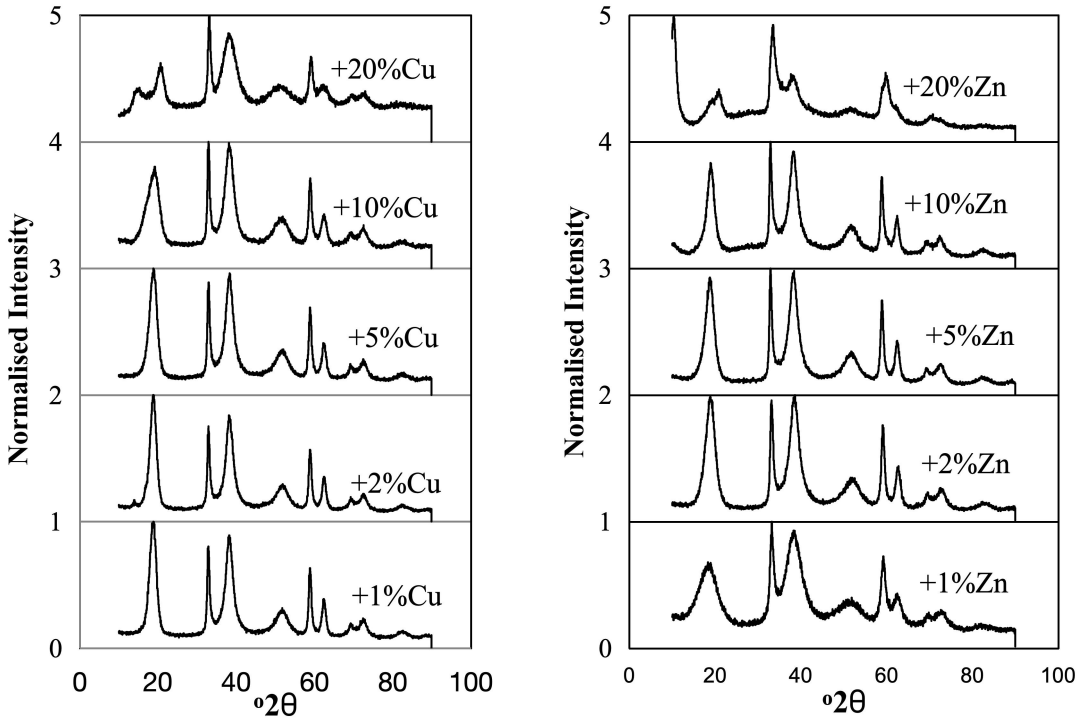

Fig.-4: XRD Patterns of $Ni(OH)_2$ Doped with Cu and Zn (1–20%), Showing Peak Shifts, Broadening, and Secondary Phases at Higher Concentrations

As shown in the Fig.-4, that nickel hydroxide typically crystallizes in the β-phases, and its XRD spectra show sharp reflections from planes such as (001), (100), and (101); when doped with copper or zinc at levels of 1–2%, the spectra remain close to pure $Ni(OH)_2$ with only slight peak broadening and minor shifts to lower angles due to lattice expansion from the larger ionic radii of Cu^{2+} and Zn^{2+}, while at 5% doping the broadening becomes more pronounced, peak intensity decreases, and weak secondary reflections may appear, indicating the onset of dopant segregation; at 10% doping, the shifts are clearer (≈0.3–0.5°), crystallinity is reduced, and mixed phases such as $Cu(OH)_2$ or $Zn(OH)_2$ may coexist with $Ni(OH)_2$, suggesting the solubility limit is near; At 20% doping, the spectra show a lot of distortion, with peaks that are much wider, less defined, and clear secondary phases (CuO, ZnO, or hydroxide derivatives).

Table-3: Calculated Microstrain (ε) Values for Nickel Hydroxide Doped with Varying Levels of Copper (1%, 2%, 5%, 10%, and 20%) (in 10^{-2})

Detected Peaks	1% Cu	Detected Peaks	2% Cu	Detected Peaks	5% Cu	Detected Peaks	10% Cu	Detected Peaks	20% Cu
18.76	5.43	18.81	5.53	18.81	6.42	18.77	10.12	15.63	10.72
32.95	1.24	33.00	1.37	33.00	1.34	33.00	1.28	20.58	6.56
38.27	3.18	38.32	3.37	38.31	3.55	38.27	3.97	33.18	1.46
51.70	2.88	51.72	3.48	51.64	3.76	51.49	4.09	38.27	5.95
62.46	0.78	58.95	0.72	58.96	0.74	58.98	0.81	51.13	7.41
69.55	0.87	62.49	0.87	62.47	1.00	62.41	1.33	59.13	0.93
72.49	1.21	69.62	1.05	69.51	0.94	69.45	1.26	62.10	2.92
82.06	10.67	72.48	1.09	72.45	1.24	72.47	1.23	71.14	3.64
		82.49	0.41	82.43	0.48	82.30	0.65		

This shows that the phases are separating and the dopant is not being incorporated as well. Overall, low doping keeps the β-$Ni(OH)_2$ structure with lattice expansion, moderate doping adds strain and lowers crystallinity, and high doping causes phase segregation. Cu improves conductivity through redox activity,

while Zn improves stability but lowers conductivity. This makes 5–10% doping the best balance between structural modification and phase purity.

The (001) reflection at 18–20° 2θ (Table-3), which represents the distance between the layers in the brucite-type structure, changes in a predictable way as the amount of Cu doping goes up. The microstrain (ε) associated with this peak increases from 5.43 (1% Cu) to 10.12 (10% Cu), indicating that the addition of Cu induces significant uneven lattice strain along the crystallographic axis. This is likely due to changes in ionic radius and/or local Jahn-Teller distortions. The considerable shift of this peak to 20.58° 2θ (ε = 6.56) at 20% Cu doping suggests that the solid solution limit may be reached, that phase segregation may begin, or that the interlayer area may undergo a large rearrangement. This makes it impossible to make a straight linear comparison with lower doping levels. Also, the appearance of a new, clear low-angle peak at about 15.63° (strain: 10.72) in the 20% Cu sample is an important sign that a new phase is forming. This could be a copper-rich layered double hydroxide (LDH) with more space between the layers, a separate copper hydroxide phase (like gerhardtite, $Cu_2(OH)_3NO_3$)[30], or a very disordered/expanded α-$Ni(OH)_2$-type structure.

Table-4: Calculated Microstrain (ε) Values for Nickel Hydroxide Doped with Varying Levels of Zinc (1%, 2%, 5%, 10%, and 20%) (in 10^{-2})

Detected Peaks	1% Zn	Detected Peaks	2% Zn	Detected Peaks	5% Zn	Detected Peaks	10% Zn	Detected Peaks	20% Zn
18.29	15.79	18.90	7.37	18.77	6.79	19.00	5.79	10.34	7.21
33.28	1.96	33.26	1.43	33.01	1.30	33.04	1.55	28.02	171.20
38.33	6.45	38.50	4.20	38.29	3.87	38.24	4.00	33.53	110.09
50.95	8.93	51.81	4.41	51.61	3.88	51.65	3.61	37.35	1.85
59.24	1.08	59.17	0.78	58.95	0.71	58.94	0.72	51.94	4.69
62.32	2.18	62.65	1.06	62.45	0.96	62.38	0.96	59.80	2.75
69.90	1.91	69.75	1.10	69.53	1.00	69.68	1.03	59.80	1.89
72.87	1.37	72.68	1.27	72.43	1.21	72.40	0.95		
		82.99	0.00	82.56	0.00	82.43	0.08		

Table-4 shows that the positions of primary reflections change systematically as the amount of Zn increases. For example, (001) moves to about 19°, (100) and (101) move to the 32–38° range, and (102), (110), and (111) move to higher angles. These shifts show that Ni^{2+} (0.69 Å, high-spin, octahedral) has been replaced by Zn^{2+} (0.74 Å, octahedral), which makes the unit cell grow. The direction and size of the shift for each reflection give us specific information about how the lattice is distorted in different ways. In a low-doping regime (1–5% Zn), most reflections show a general decrease in microstrain. For example, ε for the (001) peak goes down from about 15.79 (1% Zn) to about 6.79 (5% Zn). This shows that adding dilute Zn can make the crystal lattice more uniform, possibly by filling in cationic vacancies or fixing defects that are already there, which would make the local structure more coherent. For high doping levels (10–20% Zn), microstrain values stay low at 10% Zn, which means that the solid solution stays stable. However, at 20% Zn, there is a huge increase in microstrain for some reflections, such as ε ~171.20 at ~28.02° and ~110.09 at ~33.53°. This order-of-magnitude rise means that the lattice is very badly broken up in one area. This is in line with going over the solid solubility limit of Zn in β-$Ni(OH)_2$, which probably starts phase segregation, the formation of secondary phases (like ZnO or ε-$Zn(OH)_2$), or the loss of long-range crystallographic order. A new, low-intensity reflection shows up at about 10.34° 2θ only in the 20% Zn sample. This means that the d-spacing is about twice as large as that of the β-$Ni(OH)_2$ (001) plane. This characteristic suggests either: (a) an interlayer-expanded phase, potentially resulting from Zn-induced water intercalation or hydroxyl ordering, or (b) the emergence of a distinct layered zinc hydroxide phase exhibiting a greater basal spacing. The presence of this peak alongside significantly broadened parent-phase peaks robustly corroborates scenario (b): phase separation at elevated doping concentrations.

CONCLUSION

This research demonstrates the feasibility of an efficient phosphoric acid-based technique for extracting nickel from lateritic ore and generating doped nickel hydroxide battery materials. Taguchi analysis

determined the optimal extraction conditions by reconciling efficiency with user-friendliness. After looking more closely at the structure of Cu- and Zn-doped β-$Ni(OH)_2$ materials, it was discovered that there is a key doping threshold. For both dopants, concentrations of 10% or less facilitated the formation of a stable, coherent solid solution. Zn, in particular, made the inherent microstrain a lot lower. But when the doping level reached 20%, the system went over the limit for solid solubility. High microstrain and the appearance of extra, low-angle diffraction peaks that showed the formation of a secondary phase, like layered double hydroxides or separate metal hydroxides, proved this. These results provide a direct, structurally informed method for processing materials, employing controlled doping (<10%) to alter the lattice properties of nickel hydroxides for enhanced electrochemical stability, whereas excessive doping results in detrimental phase segregation, thereby setting a practical constraint for material design in nickel-based alkaline batteries.

ACKNOWLEDGMENTS

The authors wish to convey their heartfelt appreciation to the Ministry of Higher Education, Science, and Technology of Indonesia for aiding this research via the Research Grant Scheme [Grant No. SP DIPA-139.04.1.693320/2025 Date 30 April 2025]. Special thanks are also extended to SWD for providing DKW with access to his lab, performing the doping experiments, as well as facilitating XRD analysis, and to the Integrated Laboratory of Materials Characterisation at Universitas Tadulako for providing access to AAS, SEM and EDS facilities.

CONFLICT OF INTERESTS

The authors state that they do not have any disclosed financial interests or personal connections that might have seemed to affect the work presented in this paper.

AUTHOR CONTRIBUTIONS

The present work is related to *SDG-9: Industry, Innovation, and Infrastructure.* All the authors contributed significantly to this manuscript, participated in reviewing/editing and approved the final draft for publication. The research profile of the authors can be verified from their ORCID ids, given below:

D. K. Walanda http://orcid.org/0000-0003-4821-9514
M. Napitupulu http://orcid.org/0000-0002-0089-3115
D. Poba https://orcid.org/0000-0002-4353-2395
Y. Nurmayanti https://orcid.org/0009-0008-6474-6633
Reny https://orcid.org/0009-0008-5401-4084
S. W. Donne https://orcid.org/0000-0001-9389-7870

Open Access: This article is distributed under the terms of the Creative Commons Attribution 4.0 International License (http://creativecommons.org/licenses/by/4.0/), which permits unrestricted use, distribution, and reproduction in any medium, provided you give appropriate credit to the original author(s) and the source, provide a link to the Creative Commons license, and indicate if changes were made.
Cite this article as: D. K. Walanda *et al.*, *Rasayan J. Chem.*, 19(3), 1566-1573(2026), https://doi.org/10.31788/RJC.2026.1939662

REFERENCES

1. A. Taniguchi, N. Fujioka, M. Ikoma, and A. Ohta, *Journal of Power Sources,* **100**, 117(2001), https://doi.org/10.1016/s0378-7753(01)00889-8
2. Y. Morioka, S. Narukawa, and T. Itou, *Journal of Power Sources,* **100**, 107(2001), https://doi.org/10.1016/s0378-7753(01)00888-6
3. A. Shukla, S. Venugopalan, and B. Hariprakash, *Journal of Power Sources,* **100**, 125(2001), https://doi.org/10.1016/s0378-7753(01)00890-4
4. X. Liu, and L. Yu, *Journal of Power Sources,* **128**, 326(2004), https://doi.org/10.1016/j.jpowsour.2003.10.006
5. W. H. Zhu, J. J. Ke, H. M. Yu, and D. J. Zhang, *Journal of Power Sources,* **56**, 75(1995), https://doi.org/10.1016/0378-7753(95)80011-5
6. K. Watanabe and N. Kumagai, *Journal of Power Sources,* **76**, 167(1998), https://doi.org/10.1016/S0378-7753(98)00150-5

7. Y. Zhang, Z. Zhou, and J. Yan, *Journal of Power Sources,* **75**, 283(1998), https://doi.org/10.1016/S0378-7753(98)00111-6
8. D. S. Hall, D. J. Lockwood, C. Bock, and B. R. MacDougall, *Proceedings of the Royal Society A: Mathematical, Physical and Engineering Sciences* **471**(2015), https://doi.org/10.1098/rspa.2014.0792
9. G. Sakai, M. Miyazaki, and T. Kijima, *Journal of The Electrochemical Society,* **157**, A932(2010), https://doi.org/10.1149/1.3446847
10. A. Delahaye-Vidal, B. Beaudoin, and M. Figlarz, *Reactivity of Solids,* **2**, 223(1986), https://doi.org/10.1016/0168-7336(86)80085-7
11. K. J. Vetter and N. Jaeger, *Electrochimica Acta,* **11**, 401(1966), https://doi.org/10.1016/0013-4686(66)80018-X
12. C. Faure, Y. Borthomieu, C. Delmas, et M. Fouassier, *Journal of Power Sources,* **36**, 113(1991), https://doi.org/10.1016/0378-7753(91)80008-L
13. M. V. Vázquez, M. J. J. Avena, C. P. P. De Pauli, *Electrochimica Acta,* **40**, 907(1995), https://doi.org/10.1016/0013-4686(93)E0033-I
14. S. Deabate, F. Fourgeot, and F. Henn, *Ionics,* **5**, 371(1999), https://doi.org/10.1007/BF02376001
15. A. Delahaye-Vidal, and M. Figlarz, *Journal of Applied Electrochemistry,* **17**, 589(1987), https://doi.org/10.1007/BF01084134
16. P. Oliva, J. Leonardi, J. F. F. Laurent, C. Delmas, J. J. J. Braconnier, M. Figlarz, F. Fievet et A. d. de Guibert, *Journal of Power Sources,* **8**, 229(1982), https://doi.org/10.1016/0378-7753(82)80057-8
17. S. Le Bihan, and M. Figlarz, *Journal of Crystal Growth,* **13–14**, 458(1972), https://doi.org/10.1016/0022-0248(72)90280-1
18. R. S. McEwen, *The Journal of Physical Chemistry,* **75**, 1782(1971), https://doi.org/10.1021/j100681a004
19. B. Mani, and J. P. de Neufville, *Materials Research Bulletin,* **19**, 377(1984), https://doi.org/10.1016/0025-5408(84)90180-6
20. S. Cabanas-Polo, K. S. Suslick y A. J. Sanchez-Herencia, *Ultrasonics Sonochemistry,* **18**, 901(2011), https://doi.org/10.1016/j.ultsonch.2010.11.017
21. M. Rajamathi and P. V. Kamath, *Materials Letters,* **57**, 2390(2003), https://doi.org/10.1016/S0167-577X(02)01240-5
22. P. Vishnu Kamath, *Journal of Power Sources,* **45**, 263(1993), https://doi.org/10.1016/0378-7753(93)87017-W
23. International Energy Agency: IEA, "Critical Minerals Market Review 2023" (2023), https://doi.org/10.1787/9cdf8f39-en
24. J. Fraser, J. Anderson, J. Lazuen, Y. Lu, O. Heathman, N. Brewster, J. Bedder, and O. Masson, JRC123439, Luxembourg, (2021), https://doi.org/10.2760/212807
25. I. European Commission: Directorate-General for Internal Market Entrepreneurship and SMEs, M. Grohol, and C. Veeh, Publications Office of the European Union, (2023), https://doi.org/doi/10.2873/725585
26. M. Z. Mubarok and J. Lieberto, *Procedia Earth and Planetary Science,* **6**, 457(2013), https://doi.org/10.1016/j.proeps.2013.01.060
27. Wirawan and R. T. Jayanti. *Faculty of Industrial Technology International Congress*, **43**(2020)
28. T. Agacayak and A. Aras, *Selcuk University Journal of Engineering, Science and Technology,* **5**, 341(2017), https://doi.org/10.15317/scitech.2017.94
29. G. K. Williamson and W. H. Hall, *Acta Metallurgica,* **1**, 22(1953), https://doi.org/10.1016/0001-6160(53)90006-6
30. B. Bovio and S. Locchi, *Journal of Crystallographic and Spectroscopic Research,* **12**, 507(1982), https://doi.org/10.1007/BF01160904

[RJC-9662/2025]